mathematics

MDPI

Article

Activation Energy Performance through Magnetized Hybrid Fe_3O_4–PP Nanofluids Flow with Impact of the Cluster Interfacial Nanolayer

M. Zubair Akbar Qureshi [1,†], Qadeer Raza [1], Aroosa Ramzan [1], M. Faisal [1], Bagh Ali [2], Nehad Ali Shah [3,†] and Wajaree Weera [4,*]

[1] Department of Mathematics, Air University, Multan Campus, Multan 49501, Pakistan
[2] Faculty of Computer Science and Information Technology, Superior University, Lahore 54000, Pakistan
[3] Department of Mechanical Engineering, Sejong University, Seoul 05006, Korea
[4] Department of Mathematics, Faculty of Science, Khon Kaen University, Khon Kaen 40002, Thailand
* Correspondence: wajawe@kku.ac.th
† These authors contributed equally to this work and are co-first authors.

Abstract: The current work investigated the mass and heat transfer of the MHD hybrid nanofluid flow subject to the impact of activation energy and cluster interfacial nanolayer. The heat transport processes related to the interfacial nanolayer between nanoparticles and base fluids enhanced the base fluid's thermal conductivity. The tiny particles of Fe_3O_4 and PPy were considered due to the extraordinary thermal conductivity which is of remarkable significance in nanotechnology, electronic devices, and modern shaped heat exchangers. Using the similarity approach, the governing higher-order nonlinear coupled partial differential equation was reduced to a system of ordinary differential equations (ODEs). Fe_3O_4–PPy hybrid nanoparticles have a considerable influence on thermal performance, and when compared to non-interfacial nanolayer thermal conductivity, the interfacial nanolayer thermal conductivity model produced substantial findings. The increase in nanolayer thickness from level 1 to level 5 had a significant influence on thermal performance improvement. Further, the heat and mass transfer rate was enhanced with higher input values of interfacial nanolayer thickness.

Keywords: hybrid nanofluid; heat and mass transfer flow; MHD; Fe_3O_4–PPy hybrid nanoparticles; interfacial nanolayer; activation energy

MSC: 00-01; 99-00

Citation: Qureshi, M.Z.A.; Raza, Q.; Ramzan, A.; Faisal, M.; Ali, B.; Shah, N.A.; Weera, W. Activation Energy Performance through Magnetized Hybrid Fe_3O_4–PP Nanofluids Flow with Impact of the Cluster Interfacial Nanolayer. *Mathematics* **2022**, *10*, 3277. https://doi.org/10.3390/math10183277

Academic Editor: Camelia Petrescu

Received: 15 August 2022
Accepted: 3 September 2022
Published: 9 September 2022

1. Introduction

The activation energy is concomitant with chemical reaction and has a noteworthy role in heat and mass transfer, free convective boundary layer flows in the fields of oil container engineering and geothermal reservoirs. The exploration of thermal transportation in fluid flows is an attractive topic for researchers due to its wide applications. Moreover, thermal stability and instability are in high demand in the current era. Buongiorno et al. [1] proposed the relationship in nanofluids by incorporating Brownian diffusion and thermophoresis. Gurel [2] investigated the melting heat transport of phase change materials subject to the melting boundary condition. The finite volume approach was used to obtain numerical solutions. Dhlamini et al. [3] studied the binary chemical reactions in the mixed convective flow of nanofluids with activation energy. The effects of bioconvection, changing thermal conductivity, and activation energy past an extended sheet were investigated by Chu et al. [4]. Water was regarded as a conventional fluid by Wakif et al. [5] and in this investigation the dynamics of radiative-reactive Walters-b fluid due to mixed convection conveying gyrotactic microorganisms, tiny particles experience haphazard motion, thermomigration, and Lorentz force. To further explore the precise point of hybrid nanofluid

flow, the impact of the magnetic field, heat radiation, and activation energy with a binary chemical reaction was introduced. Sreenivasulu et al. [6] investigated the influence of activation energy on the hybrid nanofluid flow via a flat plate with viscous dissipation and a magnetic field. Ramesh et al. [7] investigated the influence of thermal performance on the usual heat source/sink effect. Chemical reaction and activation energy effects are accounted for in the mass equation. Wasif et al. [8] prepared to extend cavity construction for a broader variety of purposes, beginning with the determination of cavity shape owing to the increase in heat transmission inside that selected cavity for diverse boundary conditions. Kumar et al. [9] investigated the flow of a tangent hyperbolic fluid through a transferring stretched surface. Nonlinear radiation was used to offer warm shipping properties. Activation energy indicated different elements of mass transfer. As a result of an unstable flow over a stretched surface in an incompressible rotating viscous fluid with the appearance of a binary chemical reaction and Arrhenius activation energy, Awad et al. [10] theorized that the spectral relaxation method (SRM) could be employed to evaluate the linked highly nonlinear problem of partial differential equations. Rekha et al. [11] explored the influence of a heat source/sink on nanofluid flow through a cone, wedge, and plate while utilizing a dispersion of aluminum alloys (AA7072 and AA7075) as a base nanoparticles fluid water. The activation energy and porous material are also taken into account in the simulation.

Fe_3O_4–*PPy* core–shell nanoparticles were created using polymer polypyrrole (PPy), which could be used for cancer combination therapy that is image-guided and controlled remotely after being functionalized with polyethylene glycol. The Fe_3O_4 core, which breaks down slowly in physiological conditions, is used in this system as a magnetically controlled device for cure administration as well as a magnet. Magnetic iron oxide nanoclusters were coated for a light-absorbing near-infrared resonance imaging comparison to create a multifunctional nanocomposite. Due to their remarkable function in separation technology, Fe_3O_4 NPs have been garnering a lot of attention. In addition to having exceptional catalytic and good magnetic characteristics, the nanocomposite developed using the straightforward and easily produced Fe_3O_4 NPs also exhibits good dispensability and biocompatibility [12,13]. Suri et al. [14] studied iron oxide–PPy nanocomposites as gas and moisture sensors. Sun et al. [15] reported nanoparticles of Fe_3O_4–PANI with a very thin PANI covering of the core–shell with badly improved microwave absorption properties. Zhao et al. [16] described a method for making Fe_3O_4/*PPy* nanocomposites.

Combined mass and heat transfer flows associated with chemical reactions play a crucial function in a wide range of applications, such as transport phenomena, cooling, and heating processes in electronics, binary diffusion systems, absorption reactors, polymer processing, solar energy systems, and the plastics industry. Salmi et al. [17] presented the similarity analysis through the finite element method (FEM) to investigate the non-Fourier behavior of the heat and mass transfer. Roy et al. [18] introduced a binary chemical reaction with an activation energy effect on the heat and mass transfer of a hybrid nanofluid flow over a permeable stretching surface. Oke et al. [19] presented the combined heat and mass transfer effects in the presence of magnetohydrodynamic ternary ethylene glycol-based hybrid nanofluids over a rotating three-dimensional surface with the impact of suction velocity. The unstable MHD convective flow with the heat and mass transfer characteristics for a noncompressible gelatinous electrical system was studied by Babu et al. [20]. The effects of the magnetic field on fluid flow and heat transfer rate have been documented in numerous earlier investigations [21–25]. Sreedevi et al. [26] examined heat and mass transport through a nanofluid. Salmi et al. [27] presented a unique analysis of the combined effects of Hall and ion slip currents, the Darcy–Forchheimer porous medium, and nonuniform magnetic field under the suspension of hybrid nanoparticles with heat and mass transfer aspects. Santhi et al. [28] discussed the unsteady magnetohydrodynamics heat and mass transfer analysis of a hybrid nanofluid flow over a stretching surface with chemical reaction, suction, and slip effects. Raja et al. [29] presented a novel idea of a radiative heat and mass flux 3D hybrid nanofluid, RHF. A Bayesian regularization technique based on backpropagated neural networks (BRT-BNNs) was employed to estimate the solution of the proposed model. Shah et al. [30] investigated the Numerical simulation

of a thermally enhanced EMHD flow of a heterogeneous micropolar mixture comprising (60%)-ethylene glycol (EG), (40%)-water (W), and copper oxide nanomaterials (CuO). Bidyasagar et al. [31] analyzed the unsteady laminar flow with heat and mass transfer of an incompressible and hydromagnetic Cu–Al_2O_3/H_2O hybrid nanofluid near a nonlinearly permeable stretching sheet in the presence of nonlinear thermal radiation, viscous–ohmic dissipation, and velocity slip. Further, the impacts of heat generation and absorption, chemical reactions, convective heat, and mass conditions at the boundary were also considered by Farooq et al. [32]. Oke [33] investigated the flow of gold water nanofluids across the revolving upper horizontal surface of a paraboloid of revolution. The development of nanofluids has been groundbreaking in terms of improving fluid thermal and electrical conductivity. A real convective magnetohydrodynamic flow of a Cu–engine oil nanofluid along a vertical plate that has been convectively heated was taken into consideration by Kigio et al. [34].

Cluster interfacial nanolayer is a term that refers to a vast variety of extended quasi-two-dimensional nanoobjects that have unique physical and chemical properties, ranging from liposomes and cell membranes to graphene and layered double hydroxide flakes. Tso et al. [35] examined the effects of the interfacial nanolayer on the efficient thermal conductivity of nanofluids. The suggested model gives an equation to predict the nanolayer thickness for various kinds of nanofluids. On the other hand, in the mathematical model of Murshed et al. [36], a similar issue arises. They picked a ratio of nanolayer thermal conductivity to base fluid thermal conductivity of 1.1–2.5. Acharya et al. [37] examined the hydrothermal variations of radiative nanofluid flow by the influence of nanoparticle diameter and nanolayer. Zhao et al. [38] examined molecular dynamics simulation to investigate the effect of the interfacial nanolayer structure on enhancing the viscosity and thermal conductivity of nanofluids.

Having studied the abovementioned literature, to the best of our knowledge, no study has been conducted on the estimation of heat and mass transfer for hybrid nanofluids flowing across orthogonal porous discs subject to the effects of MHD, activation energy, and cluster interfacial nanolayers on the thermal conductivity model for hybrid nanofluid flows. Motivated by the abovementioned literature's wide scope of hybrid nanoparticles and cluster interfacial nanolayers, we considered studying the present elaborate problem. To enhance the nanoparticles stability, we also considered the activation energy. Using suitable similarity transformation quantities, the governing PDEs were transformed into dimensionless ODEs. To solve the system of ODEs, the Runge–Kutta shooting technique was used to draw numerical and graphical results.

2. Formulation of Governing Equations

The momentum, energy, and concentration equations of the incompressible flow for the two-dimensional velocity field $U = [u(x, y, t), v(x, y, t)]$ of the single-phase model in the presence of chemical reactions, heat source, and activation energy were formulated. In this problem, we assumed a viscous, laminar, incompressible, time-dependent, two-dimensional flow of a hybrid nanofluid containing $Fe_3O_4 - PPy/H_2O$ through a permeable channel of breadth 2a(t). The induced magnetic field was ignored based on the presumption of a low Reynolds number. Further, the thermophysical properties of the base fluid, the single and hybrid nanofluids are expressed in Tables 1 and 2. Both walls of the channel were absorbent and could move above and below with a time-dependent rate (a′(t)). Using these assumptions, the fluid flow-governing equations for conservation of mass, linear momentums, energy, and concentration in vector form are as follows:

$$(\nabla.U = 0), \tag{1}$$

$$\rho_{hnf}\frac{DU}{Dt} + \nabla_p - \nabla.\tau = A \times R \tag{2}$$

$$(\rho c_p)_{hnf}\left(\frac{DT}{Dt}\right) + \nabla.q_c = \beta k_r^2\left(\frac{T}{T_2}\right)^n \times exp\left(\frac{-E_a}{k^*T}\right)(c - c_2) \tag{3}$$

$$\frac{DC}{Dt} - D\nabla^2.C = -k_r^2\left(\frac{T}{T_2}\right)^n \times exp\left(\frac{-E_a}{k^*T}\right)(c - c_2) \tag{4}$$

where $\frac{D}{Dt} = \frac{\partial}{\partial t} + U.\nabla$, ρ denotes density, t represents time, τ shows the extra shear stress of the fluid, p is pressure, T stands for temperature, C represents concentration, D stands for the diffusion coefficient, $A \times R = \frac{\sigma_e B_0^2}{\rho_{hnf}} U$ signifies magnetic hydrodynamics, E_a denotes activation energy, k^* represents the Boltzmann constant, k_r^2 is the chemical reaction constant, and c_p is the specific heat capacity. The heat flux (q_c) was defined by Fourier's law of conduction, $q_c = -k_{hnf}\nabla T$, and k_{hnf} is the thermal conductivity of a hybrid nanofluid. T_1 denotes the temperature of the lower channel wall and T_2 denotes the temperature of the upper channel wall shown in Figure 1. According to assumptions, the governing Equations (1)–(4) are written as [39]:

$$\frac{\partial u}{\partial x} + \frac{\partial v}{\partial y} = 0 \tag{5}$$

$$\frac{\partial u}{\partial t} + u\frac{\partial u}{\partial x} + v\frac{\partial u}{\partial y} = -\frac{p_x}{\rho_{hnf}} + \nu_{hnf}\left(\frac{\partial^2 u}{\partial x^2} + \frac{\partial^2 u}{\partial y^2}\right) - \frac{\sigma_e B_0^2}{\rho_{hnf}}u \tag{6}$$

$$\frac{\partial v}{\partial t} + u\frac{\partial v}{\partial x} + v\frac{\partial v}{\partial y} = -\frac{p_y}{\rho_{hnf}} + \nu_{hnf}\left(\frac{\partial^2 v}{\partial x^2} + \frac{\partial^2 v}{\partial y^2}\right) \tag{7}$$

$$\frac{\partial T}{\partial t} + u\frac{\partial T}{\partial x} + v\frac{\partial T}{\partial y} = \alpha_{hnf}\left(\frac{\partial^2 T}{\partial y^2}\right) + \frac{1}{(\rho_{cp})_{hnf}}\left(\beta k_r^2\left(\frac{T}{T_2}\right)^n * exp\left(\frac{-E_a}{k^*T}\right)(c - c_2)\right) \tag{8}$$

$$\frac{\partial C}{\partial t} + u\frac{\partial C}{\partial x} + v\frac{\partial C}{\partial y} = D\left(\frac{\partial^2 C}{\partial y^2}\right) - k_r^2\left(\frac{T}{T_2}\right)^n * exp\left(\frac{-E_a}{k^*T}\right)(c - c_2) \tag{9}$$

where ρ_{hnf} denotes the density of the hybrid nanofluid and σ_e represents electrical conductivity. The physical model was used in the Cartesian coordinate system (x, y), and the u and v components of velocity were plotted on the x- and y-axes, respectively. B_0 is the magnetic field strength, α_{hnf} is the coefficient of thermal diffusivity of the hybrid nanofluid, ν_{hnf} is the kinematic viscosity of the hybrid nanofluid, T_1, C_1 and T_2, C_2 represent the temperature and concentration of the lower and upper plates with $T_1 > T_2$ and $C_1 > C_2$. The mathematical expression for the kinematic viscosity of the hybrid nanofluid and the thermal diffusivity of the hybrid nanofluid are given below:

$$v_{hnf} = \frac{\mu_{hnf}}{\rho_{hnf}}, \ \alpha_{hnf} = \frac{k_{hnf}}{(\rho c_p)_{hnf}} \tag{10}$$

where $(\rho c_p)_{hnf}$ is the hybrid nanofluid's specific capacitance and k_{hnf} is the hybrid nanofluid's thermal conductivity. The heat variations inside the fluid flow are minimal, so function T^n may be represented linearly. By excluding higher-order components, T^n may be enlarged using Taylor's series concerning temperature T_2, giving the following approximation:

$$T^n = (1-n)T_2^n + nT_2^{n-1}T\left(\frac{T}{T_2}\right)^n = (1-n) + n\frac{T}{T_2} \tag{11}$$

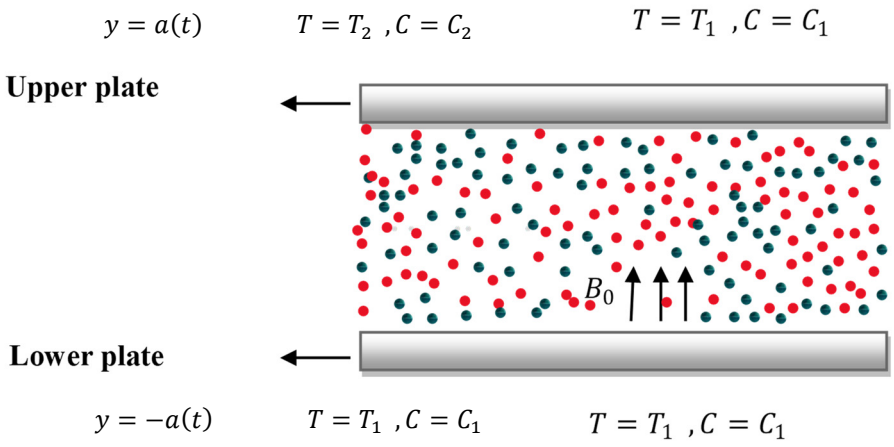

Figure 1. Physical model.

The boundary conditions of the present problem are as follows:

$$\begin{array}{l} y = -a(t)\,,\ u = 0\,,\ v = -A_1 a'(t),\ T = T_1\,,\ C = C_1 \\ y = a(t),\ u = 0\,,\ v = A_1 a'(t),\ T = T_2\,,\ C = C_2. \end{array} \tag{12}$$

The time t derivative is represented by the dash, and A is the wall permeability factor. The suitable similarity transformations are as follows:

$$\eta = \frac{y}{a}, \quad u = -\frac{x v_f}{a^2} F_\eta(\eta, t),\ v = \frac{v_f}{a} F(\eta, t),\ \theta = \frac{T - T_2}{T_1 - T_2},\ \chi = \frac{C - C_2}{C_1 - C_2} \tag{13}$$

In view of Equation (13), the continuity Equation (5) is satisfied, and Equations (6)–(9) can be written as follows:

$$\frac{v_{hnf}}{v_f} F_{\eta\eta\eta\eta} + \alpha\left(3F_{\eta\eta} + \eta F_{\eta\eta\eta}\right) + F_\eta F_{\eta\eta} - \frac{\alpha^2}{v_f} F_{\eta\eta t} - F F_{\eta\eta\eta} - \frac{\rho_f}{\rho_{hnf}} M F_{\eta\eta} = 0, \tag{14}$$

$$\begin{array}{l} \theta_{\eta\eta} + \frac{k_f}{k_{hnf}} Pr((1 - \varphi_1 - \varphi_2) + \varphi_1 \frac{(\rho c_p)_{\rho_1}}{(\rho c_p)_{hnf}} + \varphi_2 \frac{(\rho c_p)_{\rho_2}}{(\rho c_p)_{\rho_{hnf}}})(\eta\alpha - F)\theta_\eta - \frac{a^2}{\alpha_{hnf}}\theta_t + \frac{k_f}{k_{hnf}}((1 - (\varphi_1 + \varphi_2)) \\ +(\varphi_1)(\frac{\rho c_{p_{s_1}}}{\rho c_{p_{bf}}}) + (\varphi_2)(\frac{\rho c_{p_{s_2}}}{\rho c_{p_{bf}} s}))(1 + (n * \gamma)\theta[\eta])(1 - E + (E * \gamma)\theta[\eta])\chi[\eta] = 0 \end{array} \tag{15}$$

$$\chi_{\eta\eta} + Sc(\eta\alpha - F)\chi_\eta - \frac{a^2}{D}\chi_t + (Sc * \sigma)(1 + (n * \gamma)\theta[\eta])(1 - E + (E * \gamma)\theta[\eta])\chi[\eta] = 0 \tag{16}$$

Boundary conditions Equation (12):

$$\begin{array}{l} F = -Ref,,,F_\eta = 0, \quad \theta = 1,\ and\ \chi = 1,\ \ at\ \eta = -1, \\ F = Ref,\ \ ,F_\eta = 0, \quad \theta = 0,\ and\ \chi = 0,\ \ at\ \eta = 1. \end{array} \tag{17}$$

The Prandtl number is equal to $Pr = \frac{(\mu_{cp})_f}{k_f}$, $\alpha = \frac{aa'(t)}{v_f}$ is the wall expansion ratio, $\mathrm{Re} = \frac{Aaa'(t)}{v_f}$ is the permeability Reynolds number, $\gamma = \frac{T_1 - T_2}{T_2}$ is the temperature difference parameter, $\sigma = \frac{k_r^2(1-\gamma)}{a}$ is the dimensionless reaction rate, $M = \frac{\sigma_e B_0^2 a^2}{\mu_f}$ is the magnetic parameter, $E = \frac{E_a}{k^* T}$ is the dimensional activation energy parameter, $Sc = \frac{v_f}{D}$ is the Schmidt number. Finally, we set $F = fRe$ and considered the case following Majdalani et al. [40], where α is a constant, $f = f(\eta)$, $\theta = \theta(\eta)$, and $X(\eta)$, which leads to $\theta_t = 0$, $X_t = 0$, and $f_{\eta\eta\mathrm{t}} = 0$; thus, we obtained the following equation:

$$G_1 f_{\eta\eta\eta\eta} + f_{\eta\eta\eta}(\alpha\eta - Ref) + f_{\eta\eta}\left(3\alpha + Ref_\eta\right) - G_2 M Ref_{\eta\eta} = 0 \tag{18}$$

$$\theta_{\eta\eta} + G_3G_4(Pr)((\alpha\eta - Ref)\,\theta_\eta + \frac{k_f}{k_{hnf}}(Pr * \sigma * \lambda)((1 + (\gamma * n)\theta[\eta])(1 - E + (\gamma * E)\theta[\eta])\chi[\eta] = 0 \quad (19)$$

$$\chi_{\eta\eta} + Sc(\eta\alpha - Ref)\chi_\eta + (Sc*\sigma)(1 + (\gamma * n)\theta[\eta])(1 - E + (\gamma * E)\theta[\eta])\chi[\eta] = 0 \quad (20)$$

and

$$\begin{array}{llll} f = -1\,, & f_\eta = 0, & \theta = 1, & and\ \ \chi = 1, \text{at}\ \eta = -1 \\ f = 1, & f_\eta = 0, & \theta = 0, & and\ \ \chi = 0,\ \text{at}\ \eta = 1 \end{array} \quad (21)$$

where $G_1 = \left(\frac{1}{(1-(\varphi_1+\varphi_2))^{2.5}\left((1-(\varphi_1+\varphi_2))+(\varphi_1)\left(\frac{\rho_{s_1}}{\rho_{bf}}\right)+(\varphi_2)\left(\frac{\rho_{s_2}}{\rho_{bf}}\right)\right)}\right)$, $G_2 = \left(\frac{1}{\left((1-\varphi_1-\varphi_2)+\varphi_1\left(\frac{\rho_{s_1}}{\rho_{bf}}\right)+\varphi_2\left(\frac{\rho_{s_2}}{\rho_{bf}}\right)\right)}\right)$, $G_3 = \left((1-(\varphi_1+\varphi_2))+(\varphi_1)\left(\frac{\rho_{cps_1}}{\rho_{cpbf}}\right)+(\varphi_2)\left(\frac{\rho_{cps_2}}{\rho_{cpbf}}\right)\right)$, $G_4 = \left(\frac{k_{hnf}}{k_{mbf}}\frac{k_{mbf}}{k_f}\right)^{-1}$.

Table 1. Thermophysical features of a hybrid nanofluid and NPs [41].

Physical Properties	H_2O	Fe_3O_4	PPy
$\rho(kg\ m^{-3})$	997.0	5180	1.32
$C_p(J\ (kg)^{-1}K^{-1})$	4180	670	800
$K(Wm^{-1}k^{-1})$	0.6071	9.7	0.24

Table 2. Thermophysical properties of a hybrid nanofluid proposed in [42,43].

For a Nanofluid	For a Hybrid Nanofluid
$\rho_{nf} = (1-\varphi)\rho_f + \varphi\rho_p$	$\rho_{hnf} = \varphi_1\rho_{s1} + \varphi_2\rho_{s2} - (1 - \varphi_1 - \varphi_2)\rho_{bf}$
$(\rho C_p)_{nf} = (1-\varphi)(\rho C_p)_f + \varphi(\rho C_p)_p$	$\rho c_{phnf} = \varphi_1(\rho C_p)(\rho c_p)_{s1} + \varphi_2(\rho C_p)(\rho c_p)_{s2} + (1 - \varphi_1 - \varphi_2)(\rho c_p)_{bf}$
$\mu_{nf} = \frac{\mu_f}{(1-\varphi)^{2.5}}$,	$\mu_{hnf} = \frac{\mu_{bf}}{(1-\varphi_1-\varphi_2)^{2.5}}$
$k_{nf} = \frac{k_s+(N-1)k_f-(N-1)\varphi(k_{bf}-k_{s1})}{k_s+(N-1)k_f+\varphi(k_f-k_s)}k_f$	$k_{hnf} = \frac{k_{s2}+(N-1)k_{mbf}-(N-1)\varphi_{s2}(k_{mbf}-k_{s2})}{k_{s2}+(N-1)k_{mbf}+\varphi_{s2}(k_{mbf}-k_{s2})}k_{mbf}$
$\frac{k_{nf}}{kbf} = \frac{(k_{p1}-k_{nlr})\varphi_{s1}k_{nlr}(\lambda_2^2-\lambda_1^2+1)+(k_{p1}+k_{nlr})\lambda_2^2(\varphi_{s1}\lambda_1^2(k_{nlr}-k_f)+k_f)}{(\lambda_2^2(k_{p1}+k_{nlr})-(k_{p1}-k_{nlr})\varphi_{s1}(\lambda_2^2+\lambda_1^2-1))k_f}$	where $k_{mbf} = \frac{k_{s1}+(N-1)k_{bf}-(N-1)\varphi_{s1}(k_{bf}-k_{s1})}{k_{s1}+(N-1)k_{bf}+\varphi_{s1}(k_{bf}-k_{s1})}k_f$
	$\frac{k_{hnfl}}{k_{mbf}} = \frac{(k_{p2}-k_{nlr})\varphi_{s2}k_{nlr}(\lambda_2^2-\lambda_1^2+1)+(k_{p2}+k_{nlr})\lambda_2^2(\varphi_{s2}\lambda_1^2(k_{nlr}-k_{bf})+k_{bf})}{(\lambda_2^2(k_{p2}+k_{nlr})-(k_{p2}-k_{nlr})\varphi_{s2}(\lambda_2^2+\lambda_1^2-1))k_{bf}}$
	$\frac{k_{mbf}}{kf=}\frac{(k_{p1}-k_{nlr})\varphi_{p1}k_{nlr}(\lambda_2^2-\lambda_1^2+1)+(k_{p1}+k_{nlr})\lambda_2^2(\varphi_{p1}\lambda_1^2(k_{nlr}-k_f)+k_f)}{(\lambda_2^2(k_{p1}+k_{nlr})-(k_{p1}-k_{nlr})\varphi_{p1}(\lambda_2^2+\lambda_1^2-1))k_f}$

Variables φ_{s1} and φ_{s2} show volume fraction from the first and second NPs, ρ_f is the base fluid density, ρ_{s1} and ρ_{s2} are the density of the first and second solid NPs, $(\rho C_p)_{s1}$ and $(\rho C_p)_{s2}$ is the thermal capacitance of the first and second solid NPs, the thermal capacitance for the base fluid is represented as $(\rho C_p)_f$, k_{hnfl} is the effective nanolayer thermal conductivity of the hybrid nanofluid, k_f and k_{bf} represent thermal conductivity of the base fluid, $\lambda_1 = 1 + \frac{h}{r}$, $\lambda_2 = 1 + \frac{h}{2r}$, h is the nanolayer thickness, r is the radius of the particle, k_{s1} and k_{s2} are the thermal conductivities of solid nanoparticles, and k_{nlr} is the thermal conductivity nanolayer.

3. Numerical Procedure

For the determination of the existing flow model, we used the RK shooting technique. The following substitution was required to begin the process:

$$w_1 = f[\eta],\ w_2 = f'[\eta],\ w_3 = f''[\eta],\ w_4 = f'''[\eta], w_5 = \theta[\eta],\ w_6 = \theta'[\eta], w_7 = \chi[\eta],\ w_8 = \chi'[\eta] \tag{22}$$

First, in Equations (18)–(20), the model was changed in the following pattern:

$$f''''[\eta] = \frac{1}{G_1}\left((Ref[\eta] - \alpha\eta)f'''[\eta] - \left(3\alpha + Ref'[\eta]\right)f''[\eta] + G_2 M f''[\eta]\right) \tag{23}$$

$$\theta''[\eta] = -(G_3G_4(Pr(\alpha\eta - Ref[\eta])\theta'[\eta] + (Pr * \sigma * \lambda)G_4((1 + (\gamma * n)\theta[\eta])(1 - E + (\gamma * E)\theta[\eta])\chi[\eta]\ ) \tag{24}$$

$$\chi''[\eta] = -\left(Sc(\eta\alpha - Ref)\chi' + (Sc * \sigma)(1 + (n * \gamma)\theta[\eta])(1 - E + (E * \gamma)\theta[\eta])\chi[\eta]\right) \tag{25}$$

The following system was obtained by using the substitution contained in Equation (22):

$$\begin{bmatrix} w_1' \\ w_2' \\ w_3' \\ w_4' \\ w_5' \\ w_6' \\ w_7' \\ w_8' \end{bmatrix} = \begin{bmatrix} w_2 \\ w_3 \\ w_4 \\ \frac{1}{G_1}((Rew_1 - \alpha\eta)w_4 - (3\alpha + Rew_2)w_3 + G_2 M w_3) \\ w_6 \\ -(G_3G_4(Pr(\alpha\eta - Rew_1)w_6 + +(Pr * \sigma * \lambda)G_4((1 + (\gamma * n)w_5)(1 - E + (\gamma * E)w_5)w_7\ ) \\ w_7 \\ -(Sc(\eta\alpha - Rew_1)w_8 + (Sc * \sigma)(1 + (n * \gamma)w_5)(1 - E + (E * \gamma)w_5)w_7) \end{bmatrix} \tag{26}$$

Consequently, the initial condition was as follows:

$$\begin{bmatrix} w_1' \\ w_2' \\ w_3' \\ w_4' \\ w_5' \\ w_6' \\ w_7' \\ w_8' \end{bmatrix} = \begin{bmatrix} -1 \\ 0 \\ 1 \\ 0 \\ 1 \\ 0 \\ 1 \\ 0 \end{bmatrix} \tag{27}$$

The above system was solved using mathematics and a suitable initial condition. Here, the accurate Runge–Kutta shooting technique was taken into consideration. The required dimensionless ODEs can easily be tackled with this method. We obtain the initial condition by using the shooting technique in such a way that boundary conditions are satisfied and achieve the desired level of accuracy.

4. Results and Discussion

This section explains the impact of flow on suction/injection permeable Reynolds number R_e, contraction/expansion ratio parameter α, volume friction parameters φ_{s1} and φ_{s2}, magnetic parameter M, nanolayer thickness parameter h, Schmidt number Sc, exothermic/endothermic parameter λ, and dimensionless parameter n on the velocity, temperature, and concentration profiles (Figures 2–6). Figure 2 was plotted to show the effect of M on velocity profile f'. It is shown that with a rising magnetic parameter velocity, the f' component decreased. This is because by enhancing the magnetic value, Lorentz forces are produced, decreasing the axial momentum of fluid particles. We can conclude from this argument that transverse application of the magnetic field normalizes fluid velocity. The effect of E on the mass concentration profile is shown in Figure 3. It is noticed that the mass concentration profile decreased as the augmented value of the dimensionless activation energy parameter increased. The influence of nanolayer thickness on temperature is investigated and recorded in Figure 4. It is observed that the temperature decreased at the lower plate and increased at the upper plate when the value of the nanolayer thickness parameter was increased. Figure 5 depicts the influence of the volume fraction parameter on the temperature profile. It can be seen that the enhancement in volume fraction reduced the temperature in the interval $-1 < \eta < 0$ and increased in the

interval $0 < \eta < 1$. Figure 6 shows a comparison graph of effective thermal conductivity and noneffective thermal conductivity, increase in the values of volume fraction φ_{s1} and φ_{s2}; the effective thermal conductivity of hybrid nanofluids has a high heat transfer rate as compared to the non-effusive thermal conductivity of nanofluids. The reason is that noneffective thermal conductivity does not include the influence of the radius of particles and nanolayer thickness. Table 3 represents the variation in shear stress $(f''(-1))$. Physically, shear stress $(f''(-1))$ develops on the boundary of any real fluid flowing over a solid, along with liquids. According to the no-slip requirement, the float velocity has to be identical to the fluid velocity at a few stops from the boundary, even though the float velocity on the boundary has to be zero. The boundary layer is the location that lies between those spots. The shear pressure is inversely correlated with the fluid's stress rate for all Newtonian fluids in laminar float, with viscosity serving as the proportionality constant. At the bottom plate, the heat transfer rate $(\theta'(-1))$ and the mass transfer rate $(X'(-1))$ for the suction and injection instances were calculated. The flow of thermal energy between physical systems is known as heat transfer $(\theta'(-1))$. The rate of heat transfer $(\theta'(-1))$ is determined by the temperatures of the systems and the quality of the intervening medium. The mass transfer $(X'(-1))$ is a physical event that involves the observation of the net movement of generic particles from one point to another. For suction, R_e is less than zero. Suction occurs when inertia is smaller than viscosity. It was noticed that as the value of the expansion/contraction ratio parameter moved from negative to positive, it decreased the shear stress, heat, and mass transfer rate. The enhancement in the heat and mass transfer rates was noticed when the activation energy parameter was increased. It was observed that the heat transfer rate increased with the augmented values of nanolayer thickness. The Prandtl number and nanolayer thickness were opposite to the Nusselt number. The reason is that the Prandtl number is the product of diffusive momentum and the inverse of thermal diffusivity. Increasing the Prandtl number, diffusivity increases together with momentum, while the coefficient of heat flux decreases. The heat transfer rate decreases due to an increase in exothermic and endothermic parameters. It was observed that the mass transfer rate decreased with the augmented values of n. For injection $R_e > 0$ cases, injection occurred when inertia was greater than viscosity. It was observed that the effect of nanolayer thickness h and the Prandtl number had opposite impacts in both suction and injection cases on the heat transfer rate and α, E, λ, φ_{s1}, φ_{s2}, and n had the same impact in both suction and injection cases on shear stress $(f''(-1))$, $(\theta'(-1))$ and mass transfer rate $(X'(-1))$.

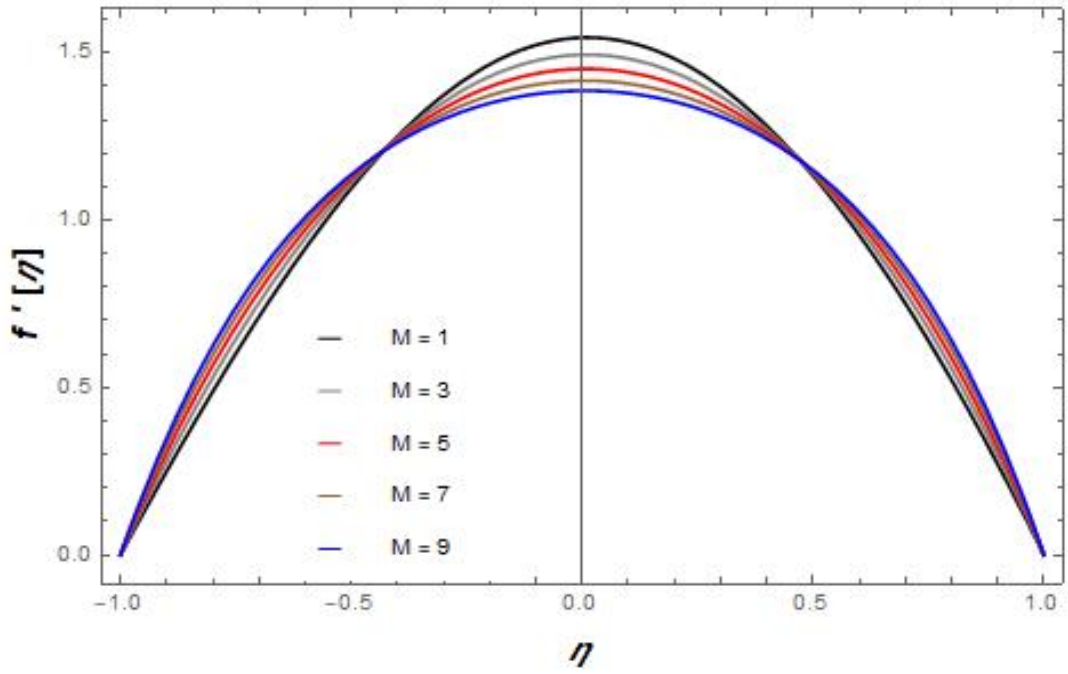

Figure 2. Effect of the magnetic parameter on velocity f'.

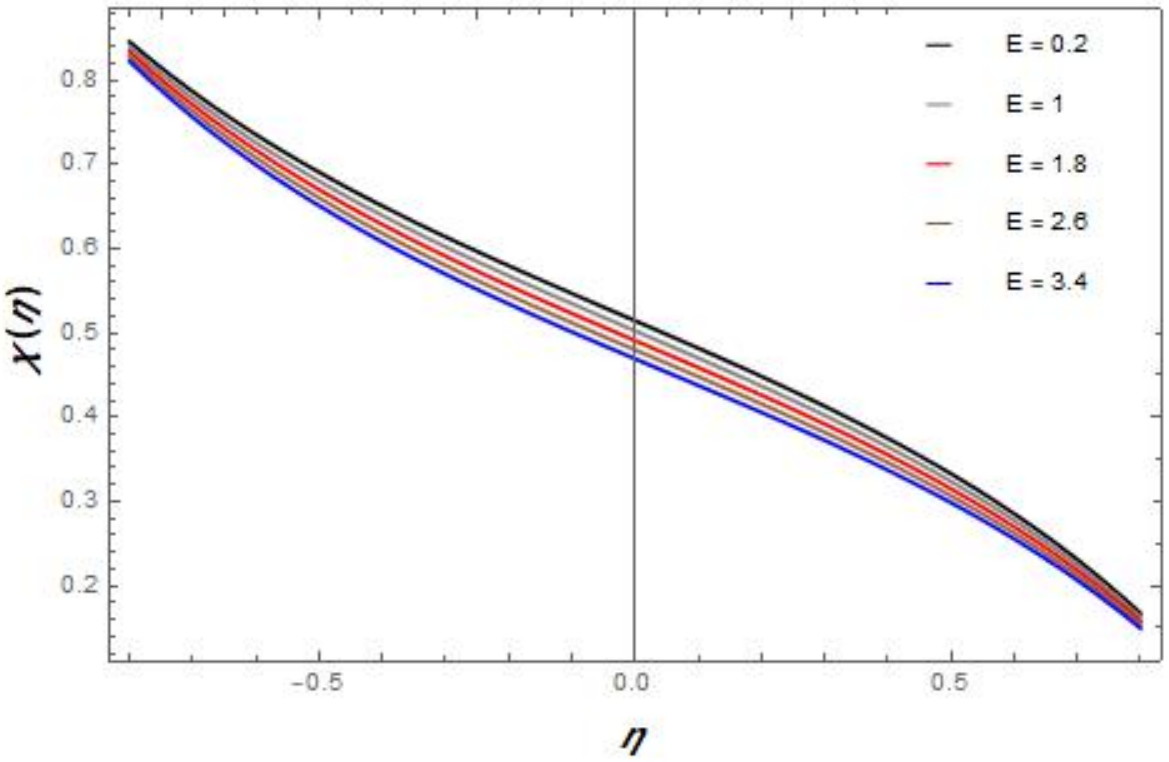

Figure 3. Effect of activation energy on mass concentration.

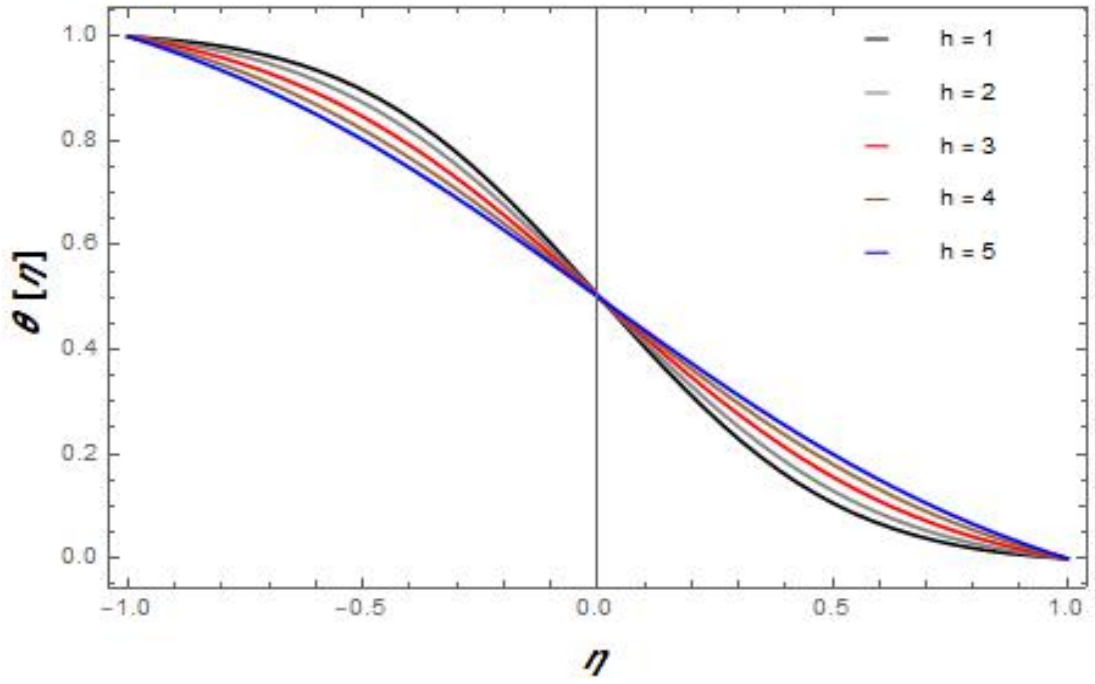

Figure 4. Effect of nanolayer thickness on the temperature profile.

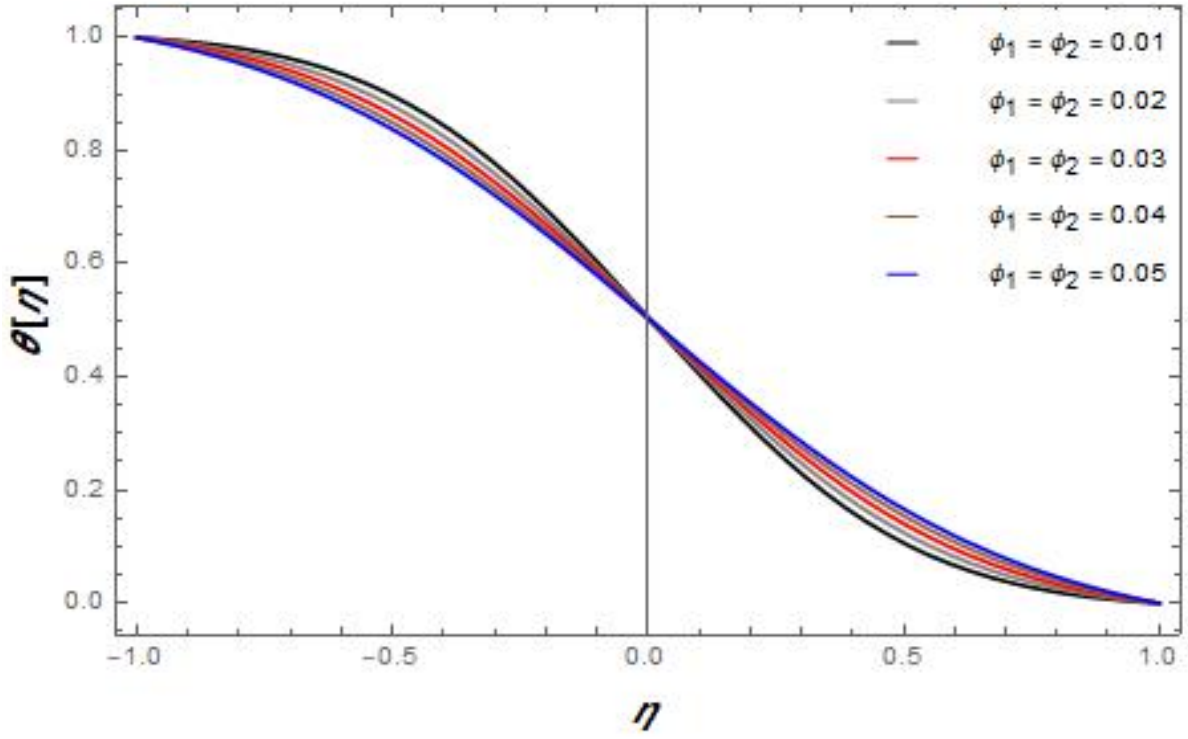

Figure 5. Effect of volume fraction on temperature.

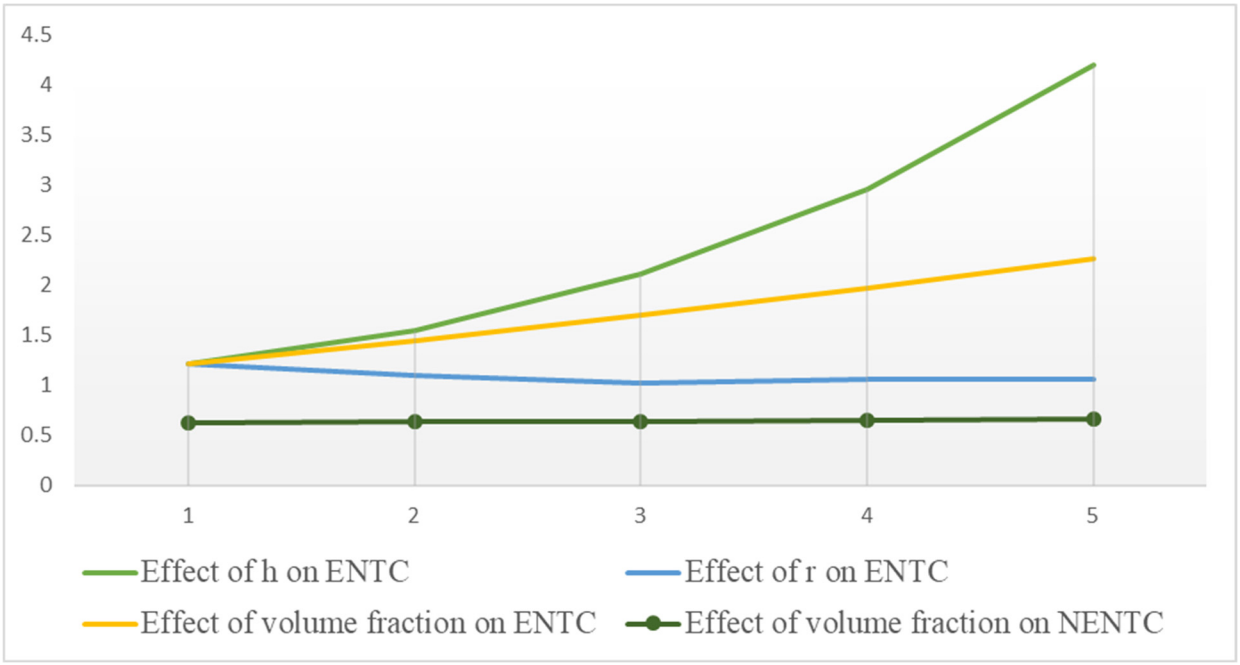

Figure 6. Effect of thermal conductivity and effective thermal conductivity.

Table 3. Variation in shear stress, heat, and mass transfer rate for suction and injection cases at the lower plate.

α	E	h	Pr	λ	n	φ_{p1}	φ_{p2}	$f''(-1)$ for the Suction Case	$\theta'(-1)$ for the Suction Case	$X'(-1)$ for the Suction Case	$f''(-1)$ for the Injection Case	$\theta'(-1)$ for the Injection Case	$X'(-1)$ for the Injection Case
−1.5						0.01	0.01	4.21559	1.80925	0.84674	4.87378	4.40691	1.52166
−1								3.77813	0.94617	0.62276	4.40357	3.20740	1.20431
0								2.94105	0.16084	0.31088	3.49395	1.18698	0.69946
1								2.16279	0.01814	0.14104	2.63460	0.24412	0.36152
1.5								1.79889	0.00558	0.09193	2.22761	0.09233	0.25207
	0.2							2.54393	0.05592	0.21175	3.05725	0.57754	0.50711
	1							2.54393	0.56180	0.22352	3.05725	0.57851	0.55284
	1.8							2.54393	0.05643	0.23519	3.05725	0.57945	0.54940
	2.6							2.54393	0.05667	0.24678	3.05725	0.58037	0.57001
	3.4							2.54393	0.05693	0.25827	3.05726	0.58128	0.59025
		1						2.54393	0.05593	0.21175	3.05725	0.57754	0.50711
		2						2.54393	0.09414	0.21175	3.05725	0.56028	0.50711
		3						2.54393	0.15128	0.21775	3.05725	0.54416	0.50711
		4						2.54393	0.21969	0.21175	3.05725	0.53125	0.50711
		5						2.54393	0.28211	0.21175	3.05725	0.52190	0.50711
			4.5					2.54393	0.1072	0.21176	3.05725	0.55586	0.50716
			5.2					2.54393	0.08231	0.21176	3.0572	0.56589	0.50711
			5.5					2.54393	0.07337	0.21175	3.05725	0.56846	0.50711
			6.1					254393	0.05593	0.21175	305725	0.57754	0.50711
			6.2					2.54393	0.05252	0.21175	3.05725	0.57754	0.50711
				1.2				2.54393	0.05252	0.21175	3.05725	0.56490	0.50711
				1.3				2.54393	0.05138	0.21175	3.05725	0.56489	0.50711
				1.7				2.54393	0.05138	0.21175	3.05725	0.56068	0.50711
				1.9				2.54393	0.05082	0.21175	3.0575	0.55857	0.50711
				2.1				2.54393	0.05025	0.21175	3.05725	0.55646	0.50711
					0.2			2.54393	0.05593	0.21175	3.05725	0.57754	0.50711
					0.3			2.54393	0.05593	0.21161	3.05725	0.57754	0.50694
					0.4			2.54393	0.05592	0.21152	3.05725	0.57757	0.50676
					0.5			2.54393	0.05592	0.21175	3.05725	0.57752	0.50659
					0.6			2.54393	0.05592	0.21175	3.05725	0.57751	0.50643
						0.02		2.05612	0.05014	0.23003	3.14578	0.08917	0.28112
						0.03		1.87661	0.04852	0.22816	2.89971	0.08710	0.25715
						0.04		1.73051	0.04646	0.22648	2.65364	0.08571	0.23846
						0.05		1.55101	0.04462	0.22419	1.30494	0.08325	0.21019
							0.02	1.99860	0.04822	0.22941	2.87560	0.10870	0.25989
							0.03	1.93061	0.04445	0.22871	2.62953	0.09875	0.24845
							0.04	1.88152	0.03947	0.22821	2.38082	0.09650	0.23587
							0.05	1.81351	0.03442	0.22751	1.88343	0.09430	0.22761

5. Conclusions

The impact of the nanolayer on the thermal conductivity of the hybrid nanofluid flow via porous surfaces is presented in this paper. In terms of shear stress, heat transfer rate, and mass transfer rate, numerical and graphical results were achieved.

- Effective nanolayer thermal conductivity indicates better results as compared to non-effective nanolayer thermal conductivity.
- Interfacial nanolayer thickness has a significant effect on the effective thermal conductivity and heat transfer rate of hybrid nanofluids.
- The heat and mass transfer rate increases with the increment in values of the interfacial nanolayer thickness and the activation energy parameter but decreases with the increase in values of particles α, Pr, and λ for the suction case.
- Shear stress is reduced with the increase in volume fraction φ_{p1}, φ_{p2} and the value of α for both cases of suction/injection.
- Mass transfer rate increase with the increment in values of the activation energy parameter.

Author Contributions: Data curation, A.R.; Formal analysis, M.F.; Funding acquisition, W.W.; Methodology, Q.R.; Software, B.A.; Validation, W.W.; Writing—original draft, M.Z.A.Q.; Writing—review & editing, N.A.S.; M.Z.A.Q. and N.A.S. contributed equally to this work and are co-first authors. All authors have read and agreed to the published version of the manuscript.

Funding: This research received funding support from the NSRF via the Program Management Unit for Human Resources & Institutional Development, Research and Innovation, (grant number B05F650018).

Institutional Review Board Statement: Not applicable.

Informed Consent Statement: Not applicable.

Data Availability Statement: The numerical data used to support the findings of this study are included within the article.

Conflicts of Interest: The authors declare no conflict of interest.

Nomenclature

B_0	Uniform magnetic field
C_p	Specific heat capacity
C	Fluid concentration
T_2	Upper plate temperature
T_1	Lower plate temperature
C_2	Upper plate concentration
C_1	Lower plate concentration
K	Dimensionless parameter
M	Magnetic parameter
Pr	Prandtl number
Re	Reynolds number
D	Diffusion coefficient
C_p	Specific heat capacity
K_r	Chemical reaction rate constant
E	Activation energy
σ	Dimensionless reaction rate
h	Nanolayer parameter
γ	Temperature difference parameter
β	Exothermic/endothermic coefficient
ρ_{hnf}	Density for the hybrid nanofluid
K_{bf}	Thermal conductivity for the base fluid
NPs	Nanoparticles
$f''(\eta)$	Shear stress

$\chi'(\eta)$	Mass transfer
μ_{bf}	Viscosity for the base fluid
ν_{hnf}	Kinematic viscosity for the hybrid nanofluid
α	Dimensionless constant
F_η	Dimensionless radial velocity profile
θ_η	Dimensionless temperature profile
σ	Thermal conductivity
V	Kinematic viscosity
μ	Dynamic viscosity
ρ	Density (kg/m^3)
ρc_p	Specific heat capacity
T	Temperature (K)
Sc	Schmidt number
$(\rho c_p)_{hnf}$	Specific heat capacity for the hybrid nanofluid
K_{hnf}	Thermal conductivity for the hybrid nanofluid
p	Pressure
μ_{hnf}	Viscosity for the HNF

References

1. Buongiorno, J.; Venerus, D.C.; Prabhat, N.; McKrell, T.J.; Townsend, J.; Christianson, R.J.; Tolmachev, Y.V.; Keblinski, P.; Hu, L.-W.; Alvarado, J.L.; et al. A benchmark study on the thermal conductivity of nanofluids. *J. Appl. Phys.* **2009**, *106*, 094312. [CrossRef]
2. GÜREL, B. A numerical investigation of the melting heat transfer characteristics of phase change materials in different plate heat exchanger (latent heat thermal energy storage) systems. *Int. J. Heat Mass Transf.* **2020**, *148*, 119117. [CrossRef]
3. Dhlamini, M.; Kameswaran, P.K.; Sibanda, P.; Motsa, S.; Mondal, H. Activation energy and binary chemical reaction effects in mixed convective nanofluid flow with convective boundary conditions. *J. Comput. Des. Eng.* **2018**, *6*, 149–158. [CrossRef]
4. Zhu, C.; Zhu, W.; Xu, L.; Zhou, X. A label-free electrochemical aptasensor based on magnetic biocomposites with Pb2+-dependent DNAzyme for the detection of thrombin. *Anal. Chim. Acta* **2018**, *1047*, 21–27. [CrossRef] [PubMed]
5. Wakif, A.; Animasaun, I.L.; Khan, U.; Shah, N.A.; Thumma, T. Dynamics of radiative-reactive Walters-b fluid due to mixed convection conveying gyrotactic microorganisms, tiny particles experience haphazard motion, thermo-migration, and Lorentz force Phys. *Scripta* **2021**, *96*, 125239. [CrossRef]
6. Sreenivasulu, M.; Vijaya, R.B. Influence of Activation Energy on the Hybrid Nanofluid Flow over a Flat Plate with Quadratic Thermal Radiation: An Irreversibility Analysis. *Int. J. Ambient. Energy* **2022**, 1–29. [CrossRef]
7. Ramesh, G.; Madhukesh, J. Activation energy process in hybrid CNTs and induced magnetic slip flow with heat source/sink. *Chin. J. Phys.* **2021**, *73*, 375–390. [CrossRef]
8. Wasif, M.; Mishal, K.A.; Haque, M.R.; Haque, M.M.; Rahman, F. Investigation of fluid flow and heat transfer for an optimized lid driven cavity shape under the condition of inclined magnetic field. *Energy Eng.* **2021**, *1*, 47–57.
9. Kumar, K.G.; Baslem, A.; Prasannakumara, B.C.; Majdoubi, J.; Rahimi-Gorji, M.; Nadeem, S. Significance of Arrhenius activation energy in flow and heat transfer of tangent hyperbolic fluid with zero mass flux condition. *Microsyst. Technol.* **2020**, *26*, 2517–2526. [CrossRef]
10. Awad, F.G.; Motsa, S.; Khumalo, M. Heat and Mass Transfer in Unsteady Rotating Fluid Flow with Binary Chemical Reaction and Activation Energy. *PLoS ONE* **2014**, *9*, e107622. [CrossRef]
11. Rekha, M.B.; Sarris, I.E.; Madhukesh, J.K.; Raghunatha, K.R.; Prasannakumara, B.C. Activation energy impact on flow of AA7072-AA7075/Water-Based hybrid nanofluid through a cone, wedge and plate. *Micromachines* **2022**, *13*, 302. [CrossRef] [PubMed]
12. Tang, S.; Lan, Q.; Liang, J.; Chen, S.; Liu, C.; Zhao, J.; Cheng, Q.; Cao, Y.-C.; Liu, J. Facile synthesis of Fe_3O_4 @PPy core-shell magnetic nanoparticles and their enhanced dispersity and acid stability. *Mater. Des.* **2017**, *121*, 47–50. [CrossRef]
13. Rehman, S.U.; Fatima, N.; Ali, B.; Imran, M.; Ali, L.; Shah, N.A.; Chung, J.D. The Casson Dusty Nanofluid: Significance of Darcy–Forchheimer Law, Magnetic Field, and Non-Fourier Heat Flux Model Subject to Stretch Surface. *Mathematics* **2022**, *10*, 2877. [CrossRef]
14. Suri, K.; Annapoorni, S.; Sarkar, A.; Tandon, R. Gas and humidity sensors based on iron oxide–polypyrrole nanocomposites. *Sens. Actuators B Chem.* **2002**, *81*, 277–282. [CrossRef]
15. Sun, Y.; Xiao, F.; Liu, X.; Feng, C.; Jin, C. Preparation and electromagnetic wave absorption properties of core–shell structured Fe3O4–polyaniline nanoparticles. *RSC Adv.* **2013**, *3*, 22554–22559. [CrossRef]
16. Zhao, H.; Huang, M.; Wu, J.; Wang, L.; He, H. Preparation of Fe_3O_4@PPy magnetic nanoparticles as solid-phase extraction sorbents for preconcentration and separation of phthalic acid esters in water by gas chromatography–mass spectrometry. *J. Chromatogr. B* **2016**, *1011*, 33–44. [CrossRef]
17. Salmi, A.; Madkhali, H.A.; Ali, B.; Nawaz, M.; Alharbi, S.O.; Alqahtani, A. Numerical study of heat and mass transfer enhancement in Prandtl fluid MHD flow using Cattaneo-Christov heat flux theory. *Case Stud. Therm. Eng.* **2022**, *33*, 101949. [CrossRef]

18. Roy, N.C.; Pop, I. Heat and mass transfer of a hybrid nanofluid flow with binary chemical reaction over a permeable shrinking surface. *Chin. J. Phys.* **2021**, *76*, 283–298. [CrossRef]
19. Oke, A.S. Heat and Mass Transfer in 3D MHD Flow of EG-Based Ternary Hybrid Nanofluid Over a Rotating Surface. *Arab. J. Sci. Eng.* **2022**, 1–17. [CrossRef]
20. Babu, B.H.; Rao, P.S.; Varma, S.V.K. Heat and Mass Transfer on Unsteady Magnetohydrodynamics (MHD) Convective Flow of Casson Hybrid Nanofluid Over a Permeable Media with Ramped Wall Temperature. *J. Nanofluids* **2022**, *11*, 552–562. [CrossRef]
21. Kakaç, S.; Pramuanjaroenkij, A. Review of convective heat transfer enhancement with nanofluids. *Int. J. Heat Mass Transf.* **2009**, *52*, 3187–3196. [CrossRef]
22. Demir, H.; Dalkilic, A.; Kürekci, N.; Duangthongsuk, W.; Wongwises, S. Numerical investigation on the single phase forced convection heat transfer characteristics of TiO_2 nanofluids in a double-tube counter flow heat exchanger. *Int. Commun. Heat Mass Transf.* **2011**, *38*, 218–228. [CrossRef]
23. Fetecau, C.; Shah, N.A.; Vieru, d. General Solutions for Hydromagnetic Free Convection Flow over an Infinite Plate with Newtonian Heating, Mass Diffusion and Chemical Reaction. *Commun. Theor. Phys.* **2017**, *68*, 768–782.
24. Ashraf, M.Z.; Rehman, S.U.; Farid, S.; Hussein, A.K.; Ali, B.; Shah, N.A.; Weera, W. Insight into Significance of Bioconvection on MHD Tangent Hyperbolic Nanofluid Flow of Irregular Thickness across a Slender Elastic Surface. *Mathematics* **2022**, *10*, 2592. [CrossRef]
25. Lou, Q.; Ali, B.; Rehman, S.U.; Habib, D.; Abdal, S.; Shah, N.A.; Chung, J.D. Micropolar Dusty Fluid: Coriolis Force Effects on Dynamics of MHD Rotating Fluid When Lorentz Force Is Significant. *Mathematics* **2022**, *10*, 2630. [CrossRef]
26. Sreedevi, P.; Reddy, P.S. Impact of Convective Boundary Condition on Heat and Mass Transfer of Nanofluid Flow Over a Thin Needle Filled with Carbon Nanotubes. *J. Nanofluids* **2020**, *9*, 282–292. [CrossRef]
27. Salmi, A.; Madkhali, H.A.; Nawaz, M.; Alharbi, S.O.; Alqahtani, A. Numerical study on non-Fourier heat and mass transfer in partially ionized MHD Williamson hybrid nanofluid. *Int. Commun. Heat Mass Transf.* **2022**, *133*, 105967. [CrossRef]
28. Santhi, M.; Rao, K.V.S.; Reddy, P.S.; Sreedevi, P. Heat and mass transfer characteristics of radiative hybrid nanofluid flow over a stretching sheet with chemical reaction. *Heat Transf.* **2020**, *50*, 2929–2949. [CrossRef]
29. Raja, M.A.Z.; Shoaib, M.; Khan, Z.; Zuhra, S.; Saleel, C.A.; Nisar, K.S.; Islam, S.; Khan, I. Supervised neural networks learning algorithm for three dimensional hybrid nanofluid flow with radiative heat and mass fluxes. *Ain Shams Eng. J.* **2021**, *13*, 101573. [CrossRef]
30. Shah, N.A.; Wakif, A.; El-Zahar, E.R.; Ahmad, S.; Yook, S.-J. Numerical simulation of a thermally enhanced EMHD flow of a heterogeneous micropolar mixture comprising (60%)-ethylene glycol (EG), (40%)-water (W), and copper oxide nanomaterials (CuO). *Case Stud. Therm. Eng.* **2022**, *35*, 102046.
31. Kumbhakar, B.; Nandi, S.; Chamkha, A.J. Unsteady hybrid nanofluid flow over a convectively heated cylinder with inclined magnetic field and viscous dissipation: A multiple regression analysis. *Chin. J. Phys.* **2022**, *79*, 38–56.
32. Farooq, U.; Lu, D.; Munir, S.; Ramzan, M.; Suleman, M.; Hussain, S. MHD flow of Maxwell fluid with nanomaterials due to an exponentially stretching surface. *Sci. Rep.* **2019**, *9*, 7312. [CrossRef] [PubMed]
33. Oke, A.S. Combined effects of Coriolis force and nanoparticle properties on the dynamics of gold–water nanofluid across nonuniform surface. *Z. Angew. Math. Mech.* **2022**, e202100113. [CrossRef]
34. Kigio, J.K.; Nduku, M.W.; Samuel, O.A. Analysis of Volume Fraction and Convective Heat Transfer on MHD Casson Nanofluid over a Vertical Plate. *Fluid Mech.* **2021**, *7*, 1–8. [CrossRef]
35. Tso, C.; Fu, S.; Chao, C.Y. A semi-analytical model for the thermal conductivity of nanofluids and determination of the nanolayer thickness. *Int. J. Heat Mass Transf.* **2014**, *70*, 202–214. [CrossRef]
36. Murshed, S.; Leong, K.; Yang, C. Thermophysical and electrokinetic properties of nanofluids—A critical review. *Appl. Therm. Eng.* **2008**, *28*, 2109–2125. [CrossRef]
37. Acharya, N.; Mabood, F.; Shahzad, S.; Badruddin, I. Hydrothermal variations of radiative nanofluid flow by the influence of nanoparticles diameter and nanolayer. *Int. Commun. Heat Mass Transf.* **2021**, *130*, 105781. [CrossRef]
38. Zhao, C.; Tao, Y.; Yu, Y. Molecular dynamics simulation of thermal and phonon transport characteristics of nanocomposite phase change material. *J. Mol. Liq.* **2021**, *329*, 115448. [CrossRef]
39. Ahmad, S.; Farooq, M.; Mir, N.A.; Anjum, A.; Javed, M. Magneto-hydrodynamic flow of squeezed fluid with binary chemical reaction and activation energy. *J. Cent. South Univ.* **2019**, *26*, 1362–1373. [CrossRef]
40. Majdalani, J.; Zhou, C.; Dawson, C.A. Two-dimensional viscous flow between slowly expanding or contracting walls with weak permeability. *J. Biomech.* **2002**, *35*, 1399–1403. [CrossRef]
41. Saba, F.; Ahmed, N.; Khan, U.; Waheed, A.; Rafiq, M.; Mohyud-Din, S.T. Thermophysical Analysis of Water Based (Cu–Al_2O_3) Hybrid Nanofluid in an Asymmetric Channel with Dilating/Squeezing Walls Considering Different Shapes of Nanoparticles. *Appl. Sci.* **2018**, *8*, 1549. [CrossRef]
42. Murshed, S.M.S.; Leong, K.; Yang, C. Investigations of thermal conductivity and viscosity of nanofluids. *Int. J. Therm. Sci.* **2008**, *47*, 560–568. [CrossRef]
43. Raza, Q.; Qureshi, M.Z.A.; Khan, B.A.; Kadhim Hussein, A.; Ali, B.; Shah, N.A.; Chung, J.D. Insight into Dynamic of Mono and Hybrid Nanofluids Subject to Binary Chemical Reaction, Activation Energy, and Magnetic Field through the Porous Surfaces. *Mathematics* **2022**, *10*, 3013. [CrossRef]